CLEAN Soil Air Water
www.clean-journal.com

Investigation of Basalt Properties as Heterogeneous Catalyst for Fenton Oxidation of Textile Wastewater

*Mohammed Saleh, Mutlu Yalvac, Hudaverdi Arslan, and Nadir Dizge**

In this study, basalt is used as a catalyst for the removal of the dyes malachite green (MG) and crystal violet (CV) from aqueous solution. First, the effect of sintering temperature on Fenton process is optimized using basalt powder. Different analysis techniques such as X-ray diffraction (XRD), X-ray fluorescence (XRF), Brunauer-Emmett-Teller (BET), and Fourier-Transform Infrared Spectroscopy (FTIR) are used to characterize basalt powder. It is concluded that Fe_2O_3 in basalt powder is the main component responsible for the degradation of dyes in the Fenton process. The maximum degradation of the dyes (97.02% for CV and 95.71% for MG) is obtained at 10 mg L^{-1} dye concentration, solution pH of 6, 1 g L^{-1} catalyst amount, and 12 mm H_2O_2 concentration for 2 h. The results are fitted to the second-order kinetic model. The reusability of the catalyst is explored, and the basalt showed stability in the removal efficiency for repeated five cycles. The degradation of real textile wastewater is also studied. The removal efficiency reached up to 60.33% at optimum conditions of pH 2, basalt amount of 5 g L^{-1}, H_2O_2 concentration of 400 mm. The results showed that the basalt powder is successfully utilized as a heterogeneous catalyst for textile wastewater treatment.

1. Introduction

The developments in the industrial sector have seriously increased the pollution of the environment.[1] Since the wastewater generated from the industrial facilities has a concentrated pollutant with very variables constituents, the treatment of industrial wastewater has become a challenge worldwide.[2] Textile industries are one of the most industrial factories that are consuming chemicals and water in large quantities.[3]

A large number of dyes are used in the textile industry. Crystal violet (CV) and malachite green (MG) are among the dyes used for dyeing textile products. CV and MG belong to the triphenylmethane dyes, which are well soluble in water.[4,5] CV enters several applications such as textiles, pH indicator, cosmetics, plastics, and paper prints.[6] The dye MG is used in the dyeing process, antiseptic, antiphrastic, antibacterial, and antifungal process.[7] Despite their wide range of uses, both dyes have toxic effects on the aquatic systems and human health.[8,9]

Sarayu and Sandhya treated textile wastewater with conventional biological treatment,[10] but the increase in the discharge standard limited this type of treatment.[11] The development of efficient processes has continued. For example, coagulation and flocculation,[12] membrane,[13] membrane bioreactor,[14] advance oxidation processes (AOPs),[15,16] and adsorption have been utilized so far.[17] For its simplicity and high efficiency, the adsorption process has been applied widely.[18] Active carbon is the most common adsorbent used for the removal of pollutants.[19] The regeneration cost of the activated carbon forced many researchers to use low-cost adsorbents in the adsorption process.[4] Besides adsorption process, advanced oxidation processes (AOPs) are used in the degradation of contaminants in the wastewater.[20] They have been used in the degradation of different types of dyes.[21,16,22] Originally, AOPs can be divided into two main categories, catalyzed and non-catalyzed processes.[23] The Fenton process is a catalyzed process that is based on the catalytic reaction of Fe^{2+} ions and hydrogen peroxide (H_2O_2) at acidic conditions (pH 2.8).[24] The reaction will produce hydroxyl and hydroperoxyl radicals that have high oxidation capacities (+2.80 and +1.42 V, respectively) to degrade dyes.[25] The limitations of this process are the need for pre- and post-treatment to adjust the pH and the second restriction is the precipitation of iron sludge.[26] The first limitation can be overcome by using heterogeneous catalysts that can achieve the reaction at neutral pH.[27] The use of materials that perform the reaction at original or neutral pH has become a priority in the AOPs.[28] Iron-oxide-based catalysts,[29,30] catalyst loaded on materials,[31,32] and zero-valent iron (ZVI)[33,34] based catalysts are used in the Fenton process. The heterogeneous Fenton catalysts still suffer from the decreases in the catalytic efficiency over multiple runs.[35,36] In addition to that, the toxicity of the released nanomaterials into the environment that may affect the living cell is still an argument topic.[37] The use of heterogeneous natural with low-cost and efficient stable material is becoming an urgent issue.

Basalt is a volcanic rock present abundantly in the earth's crest. Basalt stone is widely used in concrete aggregate, building material, paving stone, railways, decorative, and landscape

M. Saleh, M. Yalvac, H. Arslan, N. Dizge
Department of Environmental Engineering
Mersin University
Mersin 33343, Turkey
E-mail: ndizge@mersin.edu.tr

The ORCID identification number(s) for the author(s) of this article can be found under https://doi.org/10.1002/clen.202000432

DOI: 10.1002/clen.202000432

Table 1. Fundamental properties of malachite green and crystal violet dyes.

Chemical name	Malachite green	Crystal violet
Chemical structure	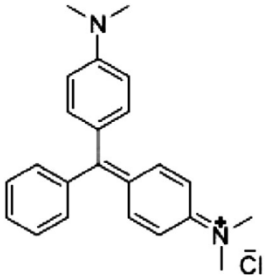	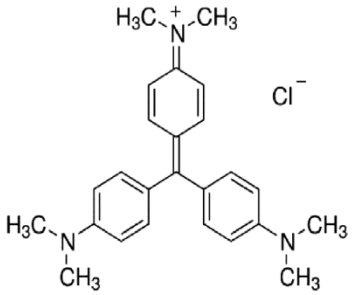
Chemical form	$C_{23}H_{25}ClN_2$	$C_{25}H_{30}N_3Cl$
Molecular weight (g mol^{-1})	346.9	407.98
UV absorption λ_{max} (nm)	618	585

applications. It is an igneous hard rock that produces a high amount of waste basalt powder material as a by-product during the processing of basalt. The waste material generated in the production facilities was used in this study. Basalt is rich in SiO_2, Al_2O_3, Fe_2O_3, and CaO elements. In this study, basalt powder was used as a catalyst for the removal of the dyes MG and CV from aqueous solution. Thermal stability, mechanical strength, resistance to the organic solvents, and the fact that it is inexpensive and readily available, have favored the use of basalt as a catalyst. The removal efficiencies of the Fenton and the adsorption were compared to determine the dominant mechanism.

2. Experimental Section

2.1. Materials

Basalt was used as the source of iron (Fe_2O_3) collected from a basalt processing plant in Osmaniye, Turkey. Hydrogen peroxide (H_2O_2, 35%, Isolab) as electron donor, hydrochloric acid (HCl, 37%, Sigma-Aldrich), and sodium hydroxide (NaOH, 98–100%, Sigma-Aldrich) for pH adjustment were used without any purification. The organic chloride salt dye MG and the cationic triphenylmethane dye CV, also named methyl violet or basic violet, were purchased from Sigma-Aldrich. The properties of the dyes are shown in **Table 1**.

2.2. Preparation of Heterogeneous Catalyst

The collected basalt was milled and sieved through 45 μm. The sieved basalt was dried at 100 °C. The obtained powder was sorted into four categories based on the sintering temperature. Raw basalt (B-R) is the powder that was not thermally treated. B-300, B-600, and B-900 are the powders sintered at 300, 600, and 900 °C, respectively. All the sintering processes were accomplished for 30 min. The temperatures were selected based on the expected chemical compositions and the crystal phase, and the sintering time was thought to be enough to track the changes. The sintering for a longer time is expected to cause agglomeration of the sintered material.

2.3. Basalt Powder Characterization

B-R, B-300, B-600, and B-900 were characterized to explore the differences between the four samples. The crystalline phases that are present in the basalt samples were analyzed by X-ray diffraction (XRD, Panalytical Empyrean). Elemental analysis was determined by X-ray fluorescence (XRF, Panalytical Zetium). The surface charges of the basalt at different pH values were measured using zeta potential (Malvern Zeta Sizer Nano ZS). The surface area, total pore volume, microporous volume, and pore diameters were measured by Brunauer–Emmett–Teller (BET) analysis (MicroActive for TriStar II Plus 2.00). The change in the functional group present on the surface of the basalt at different temperatures was scanned at wavelengths of 450–4000 cm^{-1} by Fourier transform infrared (FTIR) spectroscopy (FT/IR-6700, Jasco).

2.4. Synthetic and Real Wastewater Characterizations

Stock solutions with 100 mg L^{-1} concentration were prepared for both dyes by dissolving 0.1 g dye in 1000 mL distilled water. The stock solutions were stored in the refrigerator at 4 °C. The proposed solutions (10, 25, and 50 mg L^{-1}) were prepared from the stock solutions. The pH values were adjusted by NaOH or HCl. However, real textile wastewater was kindly provided from the textile factory in Gaziantep, Turkey. The textile wastewater had a pH value of 5.1 ± 0.2, chemical oxygen demand (COD) of 763±35 mg L^{-1}, color value of 481 ± 10 Pt-Co, and conductivity of 2.4 ± 0.5 mS cm^{-1}.

2.5. Adsorption Experiments for Malachite Green and Crystal Violet Dyes

The removal efficiencies of malachite green and crystal violet from the aqueous solutions by adsorption were investigated. The experiments were carried out in 250 mL flasks containing 100 mL solution with concentrations of 10 mg L^{-1}. From each basalt sample, 1 g L^{-1} adsorbent was inserted into the flasks. The flasks were

agitated at 155 rpm using an orbital shaker (Stuart Biolab) for 2 h at room temperature. The changes in the concentrations were measured using UV-spectrophotometry (Hach DR 3900). The removal efficiencies were calculated using Equation (1):

$$\text{Removal Efficiency (\%)} = \frac{(\text{Initial concentration} - \text{Final concentration})}{\text{Initial concentration}} \times 100 \quad (1)$$

2.6. Fenton experiments for malachite green and crystal violet dyes

The use of basalt as a heterogeneous catalyst was assessed by applying the Fenton experiments over the pH range (2-7). Different doses of basalt (0.10, 0.25, 0.50, 0.75, 1.00, 1.25, and 1.50 g L^{-1}) were added to different concentrations (10, 25, and 50 mg L^{-1}) of MG and CV in the presence of known amounts (3, 6, 9, 12, 15, and 18 mM) of H_2O_2. The solutions were shaken for 2 h at room temperature by an orbital shaker. The initial and final concentrations were measured by UV-vis spectrophotometry. The removal efficiencies of the dyes were calculated based on Equation (1).

2.6.1. The Effect of Sintering Temperature on Dye Removal Efficiency

The effect of the sintering temperature between 0 and 900 °C was investigated on the CV and MG removal of both the adsorption and the Fenton processes. 1 g L^{-1} from each sample was added to 100 mL of the CV and MG (10 mg L^{-1}) solutions. The mixtures were agitated at 155 rpm for 2 h at room temperature. For the Fenton experiments, 12 mM H_2O_2 was added to the solution before the agitation process. All the experiments were carried out at original pH value (pH 6).

2.6.2. The Effect of Solution pH on Dye Removal Efficiency

The Fenton process is significantly affected by pH. In order to explore the effects of the pH on the removal efficiencies, the solutions with 10 mg L^{-1} were prepared with different pH values (2, 2.5, 3, 4, 5, 6, and 7). The pH of each solution was adjusted by 1 M HCl or 1 M NaOH. To each solution, 1 g L^{-1} basalt was added. Then, H_2O_2 was added to the mixture followed by the agitation process.

2.6.3. The Effect of Basalt Amount on Dye Removal Efficiency

The effects of basalt amount as a heterogeneous catalyst on the degradation performances were investigated at their original pH values. The dyes initial concentration and H_2O_2 were kept constant at 10 mg L^{-1} and 12 mM H_2O_2, respectively. The agitation of the mixture continued for 2 h at room temperature. The amount of basalt was ranged from 0.25 to 2.00 g L^{-1}.

2.6.4. The Effect of H_2O_2 Concentration on Dye Removal Efficiency

The removal efficiencies of the dyes CV and MG were affected by H_2O_2. To explore that effect, pH, basalt amount, and initial concentration were kept constant at 6, 1 g L^{-1}, and 10 mg L^{-1}, respectively. The dose of H_2O_2 was ranged from 3 to 18 mM.

2.7. Kinetic Study

Zero-order, first-order, and second-order models were applied to explore the kinetic model for the removal of CV and MG by the Fenton process. The zero-order, first-order, and second-order models were fitted to the Fenton experiment results as shown in Equations (2), (3), and (4), respectively[38]:

$$C_t = C_o - k_o t \quad (2)$$

$$\ln C_t = \ln C_o - k_1 t \quad (3)$$

$$\frac{1}{C_t} = \frac{1}{C_o} + k_2 t \quad (4)$$

where C_o and C_t are the initial dyes concentration and at any time (mg L^{-1}), t is the time (min), k_o is the zero-order constant (mg L^{-1} min), k_1 and k_2 are the first-order constant (1/min) and the second-order constant (L mg^{-1} min^{-1}), respectively.

The Fenton experiments were conducted at dyes concentrations of 10, 25, 50 mg L^{-1} using 1 g L^{-1} basalt and 12 mM H_2O_2. The agitation was done at 155 rpm. To track the changes in the dye concentration, samples were taken from the solutions at appropriate time intervals.

2.8. Fenton Experiments for Real Textile Wastewater

The treatment of the collected textile wastewater by the Fenton process was tested with basalt as the catalyst. The experiments were carried out at different pH values to determine the maximum efficiency. The original pH (5.1) of the textile wastewater was adjusted to pH values in the range of 2–7. To each solution with a different pH value (2, 2.5, 3, 4, 5, 6, and 7), 5 g L^{-1} basalt, and 200 mM H_2O_2 were added and agitated (155 rpm) at room temperature for 2 h. The optimization of catalyst amount was also studied. Accordingly, basalt (1–10 g) was added to the real wastewater in the presence of H_2O_2 (500 mM) at pH 2 and agitated for 2 h at room temperature. To determine the optimum H_2O_2 concentration, six different basalt doses (1-6 g L^{-1}) were added to six distinct flasks containing 5 g L^{-1} basalt at pH 2. Color removal from real wastewater was calculated based on the wavelength scanning to determine the absorbance peaks at three different wavelengths (436, 525, and 620 nm named λ_{436}, λ_{525}, and λ_{620}).

3. Result and Discussion

3.1. Characterization of Basalt Powder

The XRD patterns for the samples are shown in **Figure 1**A. The peaks in the B-R sample were related to three main components, quartz low, hematite, and magnesium oxide. The mineral quartz with the chemical formula SiO_2 has a hexagonal crystal (PANICSD: 98-001-6336) with a space group of (P 3 1 2 1). The lattice parameters were $a = b = 4.7040$ Å, $c = 5.2610$ Å. The XRD pattern for the hematite matches the hexagonal phase of Fe_2O_3 (PANICSD: 98-002-2505) with the R-3C space group. The lattice

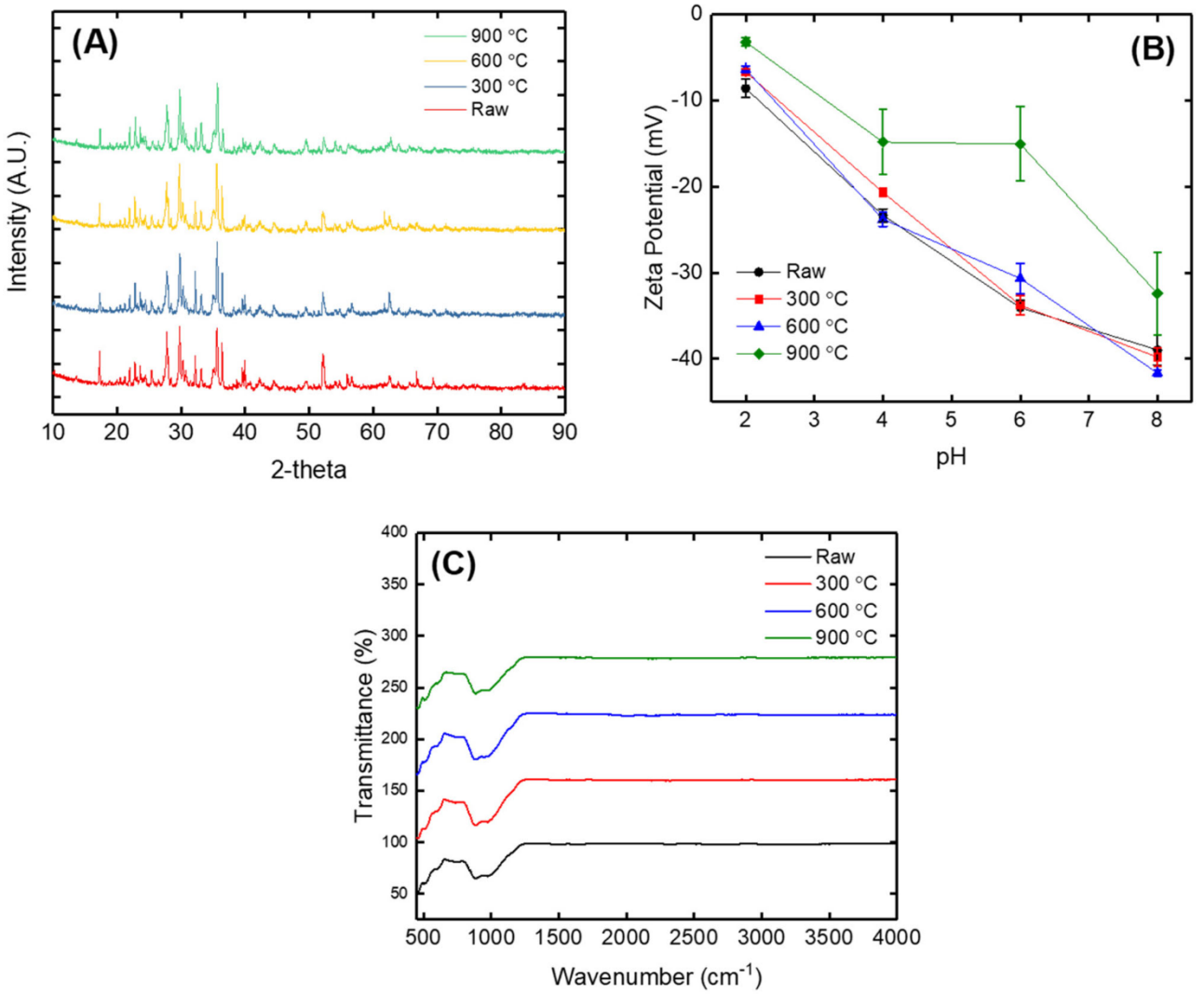

Figure 1. A) X-ray diffraction patterns; B) zeta potential; C) FTIR analysis for the basalt powder samples.

parameter values for *a* and *b* were 5.0340 Å, while for *c* = 13.7480 Å. Magnesium oxide (MgO) had a cubic phase (F m -3 m space group) with a lattice parameter *a* = 3.9610 Å (PANICSD: 98-015-7527). With the increase in the sintering temperature (B-300), magnesium oxide became unstable (hexagonal with P63/mmc space group-PANICSD: 98-018-1457). The lattice parameters of the unstable compound were *a* = *b* = 2.9990 Å, *c* = 29.7870 Å. The other compounds (quartz low and hematite) have not changed by the temperature increases. For B-600 and B-900, Periclase (chemical structure MgO) was detected (PANICSD: 98-015-9373). The crystal phase of the Periclase was cubic with *a* = 4.2640 Å. The other compounds (quartz low and hematite) have not changed by the temperature increases.

Elemental analysis was determined by XRF. The chemical compositions of the samples of basalt are shown in **Table 2**. The basalt samples consist mainly of SiO_2, Al_2O_3, MgO, Fe_2O_3, and CaO. The Fe_2O_3 increased with the increasing of the sintering temperature from 10.61% for raw basalt to 11.79% at a sintering temperature of 900 °C. Inversely, reduction in MgO and Na_2O were noted with the increases in the sintering temperature. This result supports the reduction in the MgO peaks in the XRD results, which indicates the amortization of this crystalline phase of MgO. Grassi et al. observed a similar phenomenon at the sintering process of sludge.[39] In previous studies, it has been observed that the materials used as catalysts showed a hematite percentage between 5% and 15%.[40,41] Thus, the quantity of Fe_2O_3 is high enough to use the basalt as a catalyst in this study.

The surface charges of the basalt powder samples (B-R, B-300, B-600, and B-900) were measured by dispersing them in 25 mL of distilled water. The changes in the surface charge at pH ranges of 2–8 were measured using zeta potential equipment. The changes in the surface charges for the samples are shown in Figure 1B. For all samples, the surface charges at all pH values were negative. The zeta potential decreased sharply with the increase in the pH. For the sample B-900, no change in zeta potential was noticed for pH 4–6.

Table 2. Chemical composition (wt%) for the basalt powder samples.

Compounds	B-R	B-300	B-600	B-900
Na_2O	3.16	3.16	3.11	2.61
MgO	11.64	11.69	11.55	9.89
Al_2O_3	15.39	15.46	15.43	14.77
SiO_2	44.75	44.82	45.01	44.11
P_2O_5	0.62	0.62	0.62	0.59
K_2O	1.41	1.42	1.45	1.51
CaO	8.68	8.69	8.83	9.21
TiO_2	2.03	2.04	2.08	2.21
Cr_2O_3	0.06	0.06	0.06	0.07
MnO	0.18	0.18	0.18	0.20
Fe_2O_3	10.61	10.59	10.86	11.79
LOI[a)]	1.44	1.25	0.66	0.68
Total	99.97	99.98	99.84	97.62

[a)] Loss of ignition.

Table 3. BET analysis results of basalt powder samples.

Parameter	Unit	B-R	B-300	B-600	B-900
BET surface area	$m^2\ g^{-1}$	2.7568	2.7342	1.9168	0.9035
Total pore volume	$cm^3\ g^{-1}$	0.0095	0.0075	0.0054	0.0004
Micro pore volume	$cm^3\ g^{-1}$	0.0054	0.0052	0.0037	0.0002
Pore diameter	Nm	13.7841	10.9721	11.2688	1.7709

The surface areas for the different basalt powder samples were measured using the nitrogen adsorption/desorption isotherms. In addition, the total pore volume, the micro pore volume, and the pore diameter were measured. BET analysis for the four samples is summarized in **Table 3**. The surface area of the basalt powder samples decreased with the increase in the sintering temperature. The surface area was reduced from 2.7568 $m^2\ g^{-1}$ for the B-R sample to 0.9035 $m^2\ g^{-1}$ for B-900. The total pore volume and the micro pore volume had an inverse relationship with the sintering temperature. The pore diameter reached 1.7709 nm at a sintering temperature of 900 °C.

The changes in the functional groups present on the surface of the basalt samples were analyzed by FTIR and are shown in Figure 1C. When comparing the four samples, no changes were noticed for the wavelengths 450–4000 cm^{-1}. From the results obtained in Figure 1C, the sintering temperature has no effects on the basalt functional group.

3.2. The Effect of Sintering Temperature on Dye Removal Efficiency

The effects of the sintering temperature on the removal efficiencies of the dyes CV and MG were explored. The results are shown in **Figure 2**. The removal efficiencies for both dyes by the Fenton process are higher than the adsorption process at all sintering temperatures.

For the adsorption of CV, the removal efficiency increased from 11.82% for the B-R sample to 32.91% for the B-300 sample. Then, it decreased with the increases in the sintering temperature. In general, the adsorption process is affected by the surface charge of the adsorbent. The sample B-300 had a strong negative charge, which can attract the cationic dye CV. For MG, the removal efficiency decreased with the increases in the sintering temperature. The increases in the temperature decreased the surface area, which affects the removal efficiency. The maximum adsorption was realized for B-R sample with a removal efficiency of 40.16%. The adsorption mechanism was discussed in a previous work,[42] briefly the mechanism can be summarized in Equation (5).

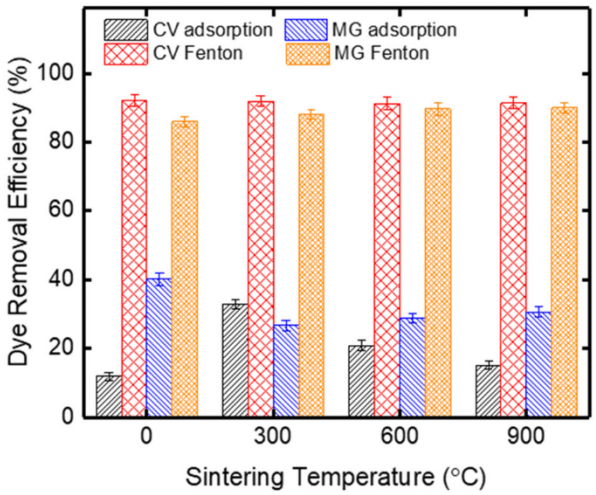

Figure 2. The effect of sintering temperature on the removal efficiencies for CV and MG (experimental conditions: basalt amount: 1 g L^{-1}, dye concentrations: 10 mg L^{-1}, agitation speed: 155 rpm, contact time: 2 h, solution pH (original pH 6) for the adsorption experiments and in addition to adsorption experiments H_2O_2 concentration: 12 mM for the Fenton experiments).

$$\text{Basalt-OH} + \text{Dye} \rightarrow \text{Basalt-OH}^- + \text{Dye}^+ \quad (5)$$

The maximum removal efficiency of CV by the Fenton process reached 97.02% for B-600 sample, while the minimum was 91.12% for B-300 sample. The Fenton process improved the removal efficiency of MG to reach 95.71% for B-600, while the minimum removal efficiency was 85.87% for B-R sample. The increases in the Fe_2O_3 percentages with the increases in the sintering temperature can explain the results. From the results seen in Figure 2, the Fenton process controls the removal efficiency of both dyes. Besides, the removal efficiency was found to be maximum at a sintering temperature of 600 °C. According to the aforementioned results, the optimization process was carried out for the Fenton process using the B-600 sample. The mechanism of the Fenton process can be summarized in Equations (6)–(10).[43]

$$Fe^{3+} + H_2O_2 \rightarrow \text{Fe-OOH}^{2+} + H^+ \quad (6)$$

$$\text{Fe-OOH}^{2+} \rightarrow HO_2^{\cdot} + Fe^{2+} \quad (7)$$

$$HO_2^{\cdot} + Fe^{2+} \rightarrow Fe^{3+} + HO_2^- \quad (8)$$

$$Fe^{3+} + HO_2^{\cdot} \rightarrow Fe^{2+} + O_2 + H^+ \quad (9)$$

$$OH^{\cdot} + H_2O_2 \rightarrow H_2O + HO_2^{\cdot} \quad (10)$$

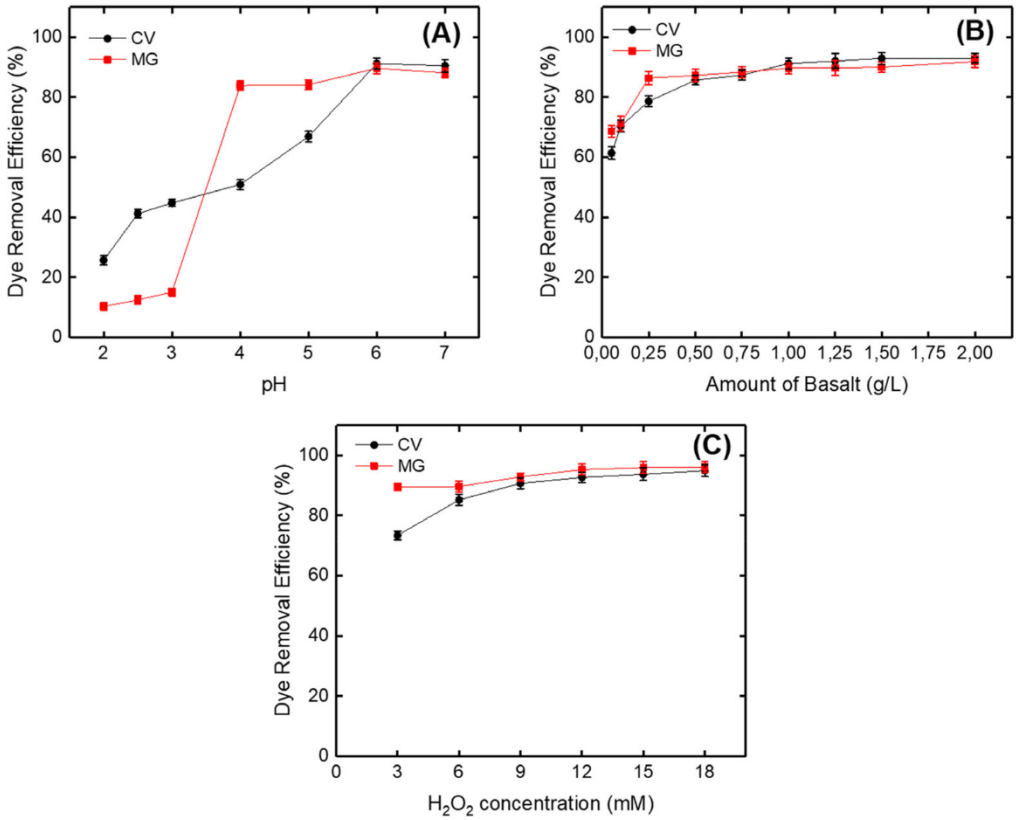

Figure 3. A) The effect of solution pH on the removal efficiencies for CV and MG dyes (experimental conditions: basalt amount: 1 g L^{-1}, dye concentrations: 10 mg L^{-1}, H_2O_2 concentration: 12 mM, agitation speed: 155 rpm, contact time: 2 h). B) The effect of basalt amount on the removal efficiencies for CV and MG dyes (experimental conditions: dye concentrations: 10 mg L^{-1}, solution pH: 6.0, H_2O_2 concentration: 12 mM, agitation speed: 155 rpm, contact time: 2 h). C) The effect of H_2O_2 on the removal efficiencies for CV and MG dyes (experimental conditions: basalt amount: 1 g L^{-1}, dye concentrations: 10 mg L^{-1}, solution pH: 6.0, agitation speed: 155 rpm, contact time: 2 h).

3.3. The Effect of Solution pH on Dye Removal Efficiency

The effects of pH on the removal efficiencies for CV and MG were explored for the Fenton process and the results are shown in **Figure 3**A. The maximum degradation percentages were obtained at original pH values. The removal efficiencies of CV and MG occurred at pH 6 with 97.02% and 95.71%, respectively. In general, the efficiencies increased with the increase in pH until the original pH value. Comparing the two dyes, the removal efficiency of CV was higher than for MG at a low pH range (2–3). Thereafter, the removal efficiency of MG dye increased sharply to reach 83.83% against 50.91% for CV at pH 4.

The photographs of the dyes before and after the Fenton process are shown in **Figure 4**. It can be clearly seen that colorless samples were obtained at the original pH (6) of the aqueous solution for both dyes.

For heterogeneous catalysts, besides the structural characterization and the chemical environment of the doped Fe species, the surface reactivity is also very important for the oxidation reaction. In addition, the role of acid–base interactions needs more attention in the use of heterogeneous Fenton catalysts.[44] Generally, the Fenton's process is not usually efficient for high pH values since hydrogen peroxide is decomposed into water and oxygen. However, the maximum removal efficiencies were obtained at pH 6 when synthetic dyes solution was used in our study. As is widely known, Fenton mechanisms significantly depend on pH, and oxidations are typically carried out at acidic conditions. At the slight acidic conditions used in this work (pH < 6), the catalyst surface was negatively charged and will adsorb/attract anions and/or positively charged ligands from the aqueous effluent.[44] Catalytic properties of metal oxides are determined by its acidity and basicity. Hydroxyl groups are present on all metal oxides surfaces. These -OH groups formed at the surface behave as Brönsted acid sites, whereas Lewis acids and Lewis bases are sites located on metallic cations and coordinately unsaturated oxygen, respectively.[45,46]

The catalytic performance of basalt powder can be affected by electrostatic interactions of dyes and basalt powder as well as interactions between metal oxides in their chemical structure. The highly dispersed iron centers included inside the silica or alumina lattice might have affected the oxidation efficiency rather than the electrostatic interaction depending on solution pH. Besides solution pH, the functional groups and charge of the catalyst surface, the functional groups nature of the dye molecules (i.e., presence of phenolic groups), and the surface charge of the solid phase can effect these interactions. Moreover,

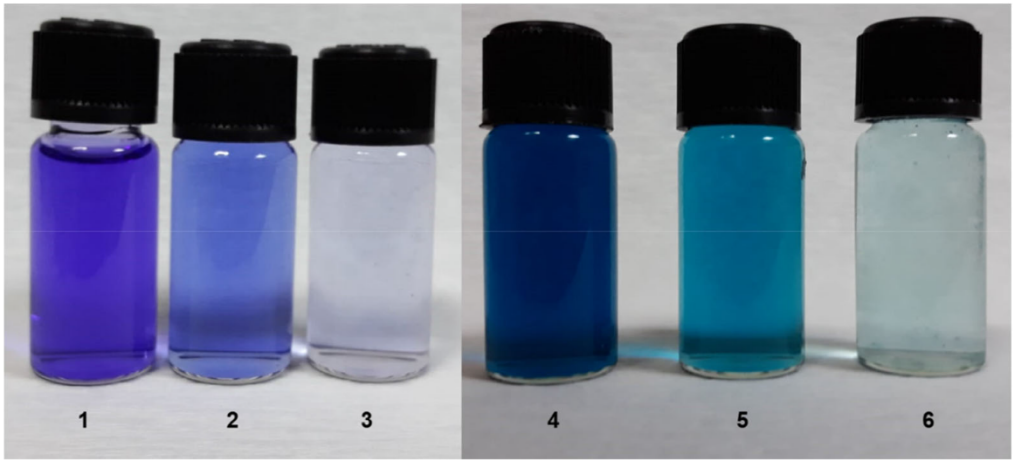

Figure 4. The photographs of the dyes before and after the Fenton process. 1) CV before Fenton, 2) CV after Fenton at pH: 2.0, 3) CV after Fenton at pH: 6.0, 4) MG before Fenton, 5) MG after Fenton at pH: 2.0, 6) MG after Fenton at pH: 6.0.

for alumina-based systems, the presence of active surface sites such as Lewis acid sites make them capable behaving as amphoteric ion exchangers depending on pH.[44] In our study, the maximum removal efficiencies were obtained at moderate acidic conditions (pH 6) due to the presence of silica and aluminum in the structure of basalt powder which can behave as ion exchangers.

3.4. The Effect of Basalt Amount on Dye Removal Efficiency

The removal efficiencies of the two dyes at different amounts of basalt powder are shown in Figure 3B. The basalt powder amount had a proportional relationship with the removal efficiency. As the basalt amount increased from 0.25 to 1 g L^{-1}, the removal efficiencies increased to 97.02% and 95.71% for CV and MG, respectively. Beyond that quantity, the removal efficiencies showed a minimal increase. Similar results were obtained in a previous work.[47] Xu et al. stated that the increases in iron beyond the optimum limit consume the hydroxyl radicals ($OH^{\bullet}$) that affecting the degradation efficiency.[48] In this study, consumption of the hydroxyl radicals was not observed with the increase in the amount of basalt powder.

3.5. The Effect of H_2O_2 Concentration on Dye Removal Efficiency

The degradation efficiencies of the dyes based on the hydrogen peroxide are shown in Figure 3C. The removal efficiency of CV increased from 73.37% at 3 mM to 97.25% at 18 mM. The removal efficiency of MG increased also from 89.39% at 3 mM to 99.25% at 18 mM. The removal efficiency increased with the increase of H_2O_2 dose, but beyond 12 mM the removal efficiency remained the same. The dose of H_2O_2 is a very important factor since the increases in the dose increases the generation of $OH^{\bullet}$. A low H_2O_2 dose limits the removal efficiency because little $OH^{\bullet}$ is generated. Similar results were obtained in previous works.[49,50]

3.6. Kinetic Study

The kinetic studies for the Fenton experiments were conducted at dye concentrations of 10, 25, 50 mg L^{-1} using 1 g L^{-1} basalt and 12 mM H_2O_2. Samples were taken during the experiment over 2 h. **Figure 5**A–D shows the fitted data for CV and MG to the linear form of the first-order and second-order model at different concentrations. Based on the correlation coefficients, the degradation of both dyes at all concentrations can be related to the second-order model. This model suggests that the hydroxyl radicals and the active sites present on the basalt surface is limited to heterogeneous Fenton of both dyes. The correlation coefficients and the rate constant for the degradation of CV and MG are shown in **Table 4**.

3.7. Reusability

The reusability of the basalt as the catalyst was examined for the CV and MG dye degradation. The experimental procedure was conducted at the optimum conditions, that is, pH 6, 18 mM H_2O_2, and 1 g L^{-1} catalyst amount. The catalyst after each experiment was collected by centrifugation. The removal efficiencies for both dyes did not change for five cycles (**Figure 6**). Thereafter, the loss of catalyst after each cycle decreased the efficiencies from 97.02% to 96.21% for CV and from 95.71% to 94.65% for MG.

3.8. Real Textile Wastewater Experiments

The experiments were carried out at different pH values to determine the maximum removal efficiency. The original pH (5) of the textile wastewater was adjusted to pH values of 2–7. For each solution with a different pH value (2, 2.5, 3, 4, 5, 6, and 7), 5 g L^{-1} basalt and 200 mM H_2O_2 were added and agitated at room temperature. As shown in **Figure 7**A, the removal efficiency of the wastewater reached the maximum at pH 2. With the increase in the pH values, the removal efficiency decreased. Similar results were obtained previously.[51]

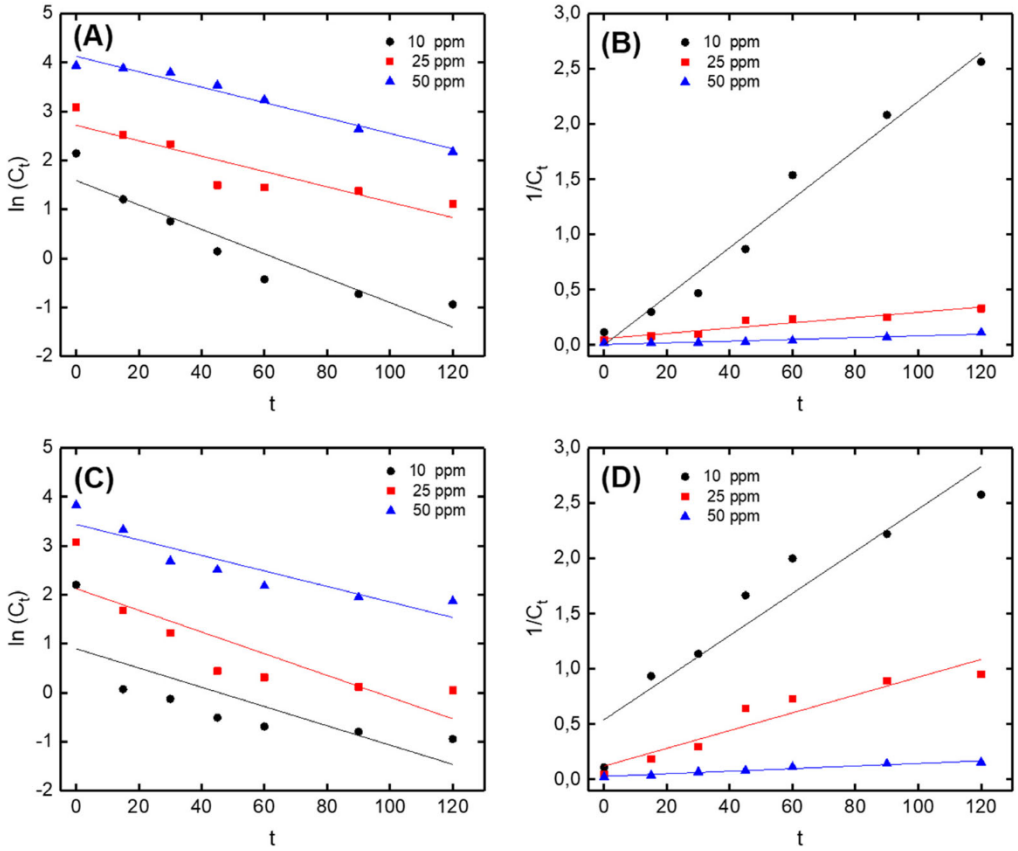

Figure 5. A) First-order model for the removal of CV, B) second-order model for the removal of CV, C) first-order model for the removal of MG, D) second-order model for the removal of MG.

Table 4. The correlation coefficients and the rate constant for degradation of CV and MG dyes.

Dye	Dye concentration [mg L^{-1}]	Decolorization [%]	Zero order		First order		Second order	
			k_o[mg L^{-1} min^{-1}]	R^2	k_1 [1/min]	R^2	k_2 [L mg^{-1} min^{-1}]	R^2
CV	10	97.02	0.0524	0.5785	0.0249	0.8793	0.0221	0.9758
	25	86.13	0.1331	0.6747	0.0157	0.8153	0.0024	0.9020
	50	82.77	0.3924	0.9683	0.0157	0.9696	0.0008	0.8949
MG	10	95.71	0.0446	0.3509	0.0197	0.5899	0.0191	0.9002
	25	95.15	0.1178	0.4444	0.0222	0.7242	0.0080	0.9035
	50	85.96	0.2789	0.6573	0.0158	0.8428	0.0012	0.9571

The optimization of the catalyst amount was also studied. Accordingly, the degradation efficiency increased from λ_{436} 12.97%, λ_{525} 18.15%, and λ_{620} 19.84% for 1 g L^{-1} basalt to λ_{436} 31.06%, λ_{525} 34.52%, and λ_{620} 34.24% for 5 g L^{-1} basalt. Beyond that amount, the degradation efficiencies decreased sharply (Figure 7B). The decreases in the efficiencies can be related to the consumption of the hydroxyl radicals by the excess H_2O_2.[47,48]

To determine the optimum of H_2O_2 dosage, six different doses were added to six distinct flasks containing 5 g L^{-1} basalt at pH 2. With the increases in H_2O_2 dosage, the generation of hydroxyl radicals increased, thus the degradation efficiency increased to 60.33% at 400 mM H_2O_2 for λ_{620} (Figure 7C). Excessive H_2O_2 acts as hydroxyl radical scavenger and lowers the degradation efficiency to 51.63% and 41.03% for dosages of 500 and 600 mM, respectively.

3.9. Comparison with Other Studies

Many researchers tried to fabricate or use the natural components as catalysts in the Fenton or Fenton-like process. El-Halil and colleagues optimized the degradation process of malachite green by the Fenton process using the Fe^{2+}/H_2O_2 combination. The maximum degradation efficiency was 93.83%.[52]

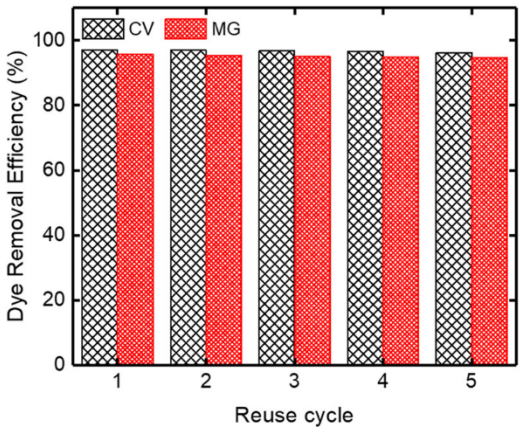

Figure 6. Reuse cycle for basalt powder catalyst for CV and MG dye degradation (experimental conditions: dye concentrations: 10 mg L^{-1}, solution pH: 6.0, H_2O_2 concentration: 12 mM, agitation speed: 155 rpm, contact time: 2 h).

Malachite green was also completely rapidly degraded by $MgFe_2O_4$ nanoparticles at a neutral pH value (pH 7).[53] The green chemistry process was utilized to prepare iron nanoparticles (Fe-NP's). Wu et al. used tea extracts for Fe-NP's preparation. The prepared nanoparticles were applied as a catalyst for malachite green degradation, where the removal efficiency exceeded 85%.[54] Meriem et al. studied the degradation of malachite green by a heterogeneous Fenton-like process using copper as a catalyst. The in-situ formation of H_2O_2/*OH decolorized the dye solution completely in 60 min.[55] The degradation of crystal violet by an iron oxide-coated granular activated carbon as a catalyst in the Fenton process reached a maximum efficiency of 71%.[56] The catalytic ozonation for the crystal violet degradation using an Fe/activated carbon catalyst was also investigated. The degradation percentage was 96% after 30 min.[57] Chen and colleagues examined the degradation of crystal violet by non-thermal plasma combined with Fe^{2+}-activated persulfate as a catalyst, where the efficiency ranged from 12.8% to 97.9%.[58] Xu et al. prepared a Mo-Cu-Fe-O composite for catalytic wet air oxidation under ambient temperature and pressure. The degradation efficiency of crystal violet reached 92.8%.[59] In this study, basalt powder was utilized as a catalyst which is rich in SiO_2, Al_2O_3, Fe_2O_3, and CaO elements. Gan and Li studied Fenton-like degradation of rhodamine B (RhB) using an iron silica catalyst.[60] They reported that the catalytic performance was improved by a rice hull-based silica loaded with iron content as low as 3 wt%. They also reported that negative effects on RhB removal were observed with the increase of cations valences. The degradation process was slowed down by divalent cations such as Mg^{2+} and Ca^{2+} compared to monovalent cations such as K^+ and Na^+. This implies that multivalent cations with stronger electrostatic attraction to the negative silica surface are more efficient in competing with RhB molecules for the adsorption on the catalyst surface. This reason may explain why we did not reach complete color removal efficiency in our study. The basalt powder was compared with other types of catalysts (**Table 5**). Accordingly,

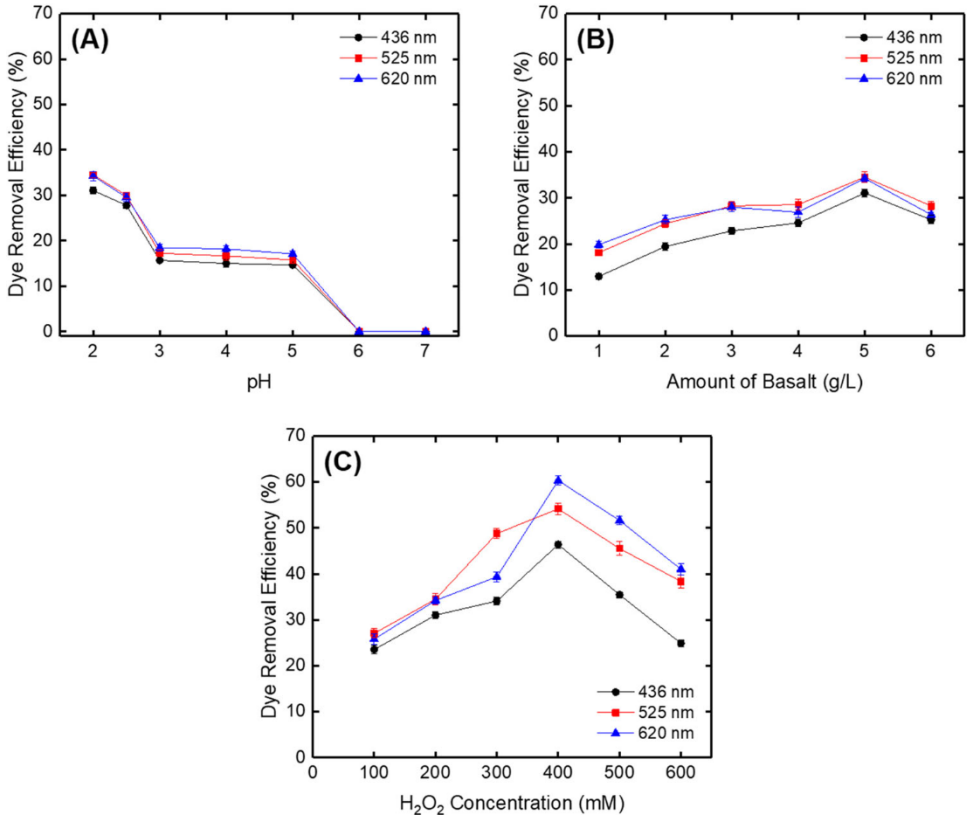

Figure 7. Decolorization efficiency of the real textile wastewater by basalt powder catalyst. A) The effect of wastewater pH, B) the effect of basalt amount, C) the effect of H_2O_2 concentration.

Table 5. Comparison with other studies using the Fenton process.

Catalyst	Optimum condition	Removal efficiency	Kinetic	Reusability	Reference
Basalt was used as a catalyst for malachite green degradation after the sintering process at 600 °C.	H_2O_2 concentration of 12 mM, catalyst dosage of 1 g L^{-1}, pH 6	10 ppm: 95.7% 25 ppm: 95.1% 50 ppm: 85.9%	Second order	5 cycles	This study
Basalt was used as a catalyst for crystal violet degradation after the sintering process at 600 °C.	H_2O_2 concentration of 12 mM, catalyst dosage of 1 g L^{-1}, pH 6	10 ppm: 97.0% 25 ppm: 86.1% 50 ppm: 82.8%	Second order	5 cycles	This study
Immobilized ferroferric oxide (Fe_3O_4) nanoparticles (NPs) with reduced graphene oxide (rGO)-based micromotors for methylene blue degradation	1.5% H_2O_2	90%	–	3 cycles	[28]
Natural pyrite particles were used as catalyst for C.I. reactive orange 29 degradaion	H_2O_2 concentration of 3 mM, catalyst dosage of 3 g L^{-1}, pH 2	10 ppm: 94%	Pseudo-first order	5 cycles	[60]
Nanoscale zero-valent iron supported on kaolinite was used to degrade acid black 1 (AB1)	pH 2, catalyst dose: 0.3 g L^{-1}, H_2O_2 concentration of 0 mM	30 ppm: 98%	Pseudo-first order	1 cycle	[61]
Basalt was used as a catalyst for methylene blue (MB) and basic red 18 (BR18) degradations.	pH 2, catalyst dose: 1 g L^{-1}, H_2O_2 concentration of 5 mM	70 ppm: 87% (MB) 70 ppm: 28% (BR18)	–	3 cycles	[42]

basalt powder has two advantages over other materials. The first is that the basalt is natural and has not been modified with any chemicals, which encourages the green engineering practices. The second advantage is the stability of the removal efficiency that is the inadequacy of the other materials.

4. Conclusion

In this study, the use of basalt as a heterogeneous catalyst for the degradation of CV and MG by the Fenton process was investigated. The results showed high performances for the removal of both dyes. The adsorption experiments were conducted to understand the degradation mechanism. The removal efficiencies for CV and MG by the Fenton process can be considered higher than the adsorption for each sintering temperature. The sintering temperature, the initial pH, the amount of basalt, and the dose of H_2O_2 were optimized. The maximum removal efficiency for both dyes occurred for B-600, the original pH (6), 1 g L^{-1} basalt dose, and 12 mM H_2O_2. The removal of CV and MG were fitted to the second-order model. The degradation of textile wastewater was also explored. The removal efficiency reached 54% at optimum conditions of pH 2, 5 g L^{-1} basalt, 400 mM H_2O_2. The difference in the degradation efficiencies between the synthetic dyes solution and the textile wastewater can be related to the uses of different types of chemicals in the production process and the presence of different types and charges of dyes in the textile wastewater. In this study, the basalt was successfully utilized as a heterogenetic catalyst for dye removal. The importance of this work can be noticed from different perspectives; the first one, that the used basalt is an industrial by-product with no commercial value. In contrast, the factories spent money to get rid of that waste. In addition to that, the use of basalt as a possible source for hematite reduced the cost of the Fenton process since the Fe ions were not added. For the synthetic dye solutions, the basalt was used as a heterogenic catalyst at different pH values, and the optimum was at origin pH, that means the use of acid/base are not necessary, which also reduces the costs. Another advantage is that the use of the Fenton process in wastewater treatment is a solution to overcome the waste sludge problem. Unfortunately, the use of basalt in textile wastewater treatment is still a challenging issue and further studies should be applied.

Conflict of Interest

The authors declare no conflict of interest.

Author Contributions

N.D.: Writing-review and editing.

Data Availability Statement

The data that support the findings of this study are available from the corresponding author upon reasonable request.

Keywords

adsorption, basalt powder, Fenton process, heterogeneous catalyst

Received: December 11, 2020
Revised: June 26, 2021
Published online: October 25, 2021

[1] B. Unal, Z. Bilici, N. Ugur, Z. Isik, E. Harputlu, N. Dizge, K. Ocakoglu, *J. Water Process. Eng.* **2019**, *32*, 100897.
[2] M. Yalvaç, H. Arslan, M. Saleh, M. Gün, M. Ş. Hekim, *Pamukkale Univ. J. Eng. Sci.* **2020**, *27*, 349.
[3] C. Holkar, A. Jadhav, D. Pinjari, N. Mahamuni, A. Pandit, *J. Environ. Manage.* **2016**, *182*, 351.
[4] M. Saleh, M. Yalvaç, H. Arslan, M. Gün, *Eur. J. Sci. Technol.* **2019**, *17*, 755.
[5] N. P. Raval, P. U. Shah, N. K. Shah, *Appl. Water Sci.* **2017**, *7*, 3407.
[6] A. Abd-Elhamid, G. Fawal, M. Akl, *Egypt. J. Chem.* **2019**, *62*, 541.
[7] M. Roosta, M. Ghaedi, N. Shokri, A. Daneshfar, R. Sahraei, A. Asghari, *Spectrochim. Acta, Part A* **2014**, *118*, 55.

[8] E. Moawed, H. Kiwaan, A. Elbaraay, *Int. J. Sci. Eng. Res.* **2019**, *1*, 1259.
[9] N. Gupta, A. K. Kushwaha, M. Chattopadhyaya, *Arab. J. Chem.* **2016**, *9*, S707.
[10] K. Sarayu, S. Sandhya, *Appl. Biochem. Biotechnol.* **2012**, *167*, 645.
[11] V. Gupta, S. Khamparia, I. Tyagi, D. Jaspal, A. Malviya, *Global J. Environ. Sci. Manage.* **2015**, *1*, 71.
[12] A. Verma, R. Dash, P. Bhunia, *J. Environ. Manage.* **2012**, *93*, 154.
[13] C. Thamaraiselvan, M. Noel, *Crit. Rev. Environ. Sci. Technol.* **2015**, *45*, 1007.
[14] V. Jegatheesan, B. Pramanik, J. Chen, D. Navaratna, C. Chang, L. Shu, *Bioresour. Technol.* **2016**, *204*, 202.
[15] W. Du, S. Chen, *J. Environ. Manage.* **2018**, *206*, 507.
[16] S. Carvalho, N. Carvalho, *J. Environ. Manage.* **2017**, *187*, 82.
[17] M. Saleh, M. Yalvaç, H. Arslan, *Karbala Int. J. Mod. Sci.* **2019**, *8*, 55.
[18] S. Khamparia, D. K. Jaspal, *J. Environ. Manage.* **2017**, *197*, 498.
[19] A. Albadarin, M. Collins, M. Naushad, S. Shirazian, G. Walker, C. Mangwandi, *Chem. Eng. J.* **2017**, *307*, 264.
[20] J. Herney-Ramirez, M. Vicente, L. Madeira, *Appl. Catal., B* **2010**, *98*, 10.
[21] C. Benatti, C. Tavares, T. Guedes, *J. Environ. Manage.* **2006**, *80*, 66.
[22] S. Abo-Farha, *J. Am. Sci.* **2010**, *6*, 128.
[23] L. Rizzo, T. Agovino, S. Nahim-Granados, M. Castro-Alf erez, P. Fernandez-Ib anez, M. Polo-Lopez, *Water Res.* **2019**, *149*, 272.
[24] J. Kim, T. Zhang, W. Liu, P. Du, J. Dobson, C. Huang, *Environ. Sci. Technol.* **2019**, *53*, 13312.
[25] J. Wang, K. Shang, X. Guo, X. Xia, L. Da, *J. Chem. Technol. Biotechnol.* **2020**, *95*, 567.
[26] N. Thomas, D. D. Dionysiou, S. C. Pillai, *J. Hazard. Mater.* **2020**, *404*, 124082.
[27] G. Wang, K. Tang, Y. Jiang, H. R. Andersen, Y. Zhang, *Bioresour. Technol.* **2020**, *318*, 124195.
[28] H. Shi, X. Chen, K. Liu, X. Ding, W. Liu, M. Xu, *J. Colloid Interface Sci.* **2020**, *572*, 39.
[29] S. Pouran, A. Aziz, A. Raman, W. Mohd, A. Wan, *J. Cleaner Prod.* **2014**, *64*, 24.
[30] Y. Zhu, R. Zhu, Y. Xi, T. Xu, L. Yan, J. Zhu, G. Zhu, H. He, *Chem. Eng. J.* **2018**, *346*, 567.
[31] X. Liu, Y. Zhou, J. Zhang, L. Tang, L. Luo, G. Zeng, *ACS Appl. Mater. Interfaces* **2017**, *9*, 20255.
[32] S. Navalon, M. Alvaro, H. Garcia, *Appl. Catal., B* **2010**, *99*, 1.
[33] S. Li, W. Wang, F. Liang, W. Zhang, *J. Hazard. Mater.* **2017**, *322*, 163.
[34] N. Ezzatahmadi, G. Ayoko, G. Millar, R. Speight, C. Yan, J. Li, S. Li, J. Zhu, Y. Xi, *Chem. Eng. J.* **2017**, *312*, 336.
[35] J. Tang, J. Wang, *Environ. Sci. Technol.* **2018**, *52*, 5367.
[36] A. Serrà, R. Artal, J. García-Amorós, E. Gómez, L. Philippe, *Chem. Eng. J.* **2020**, *388*, 124278.
[37] R. Hamers, *Acc. Chem. Res.* **2017**, *50*, 633.
[38] S. Sun, C. Li, J. Sun, S. Shi, M. Fan, Q. Zhou, *J. Hazard. Mater.* **2009**, *161*, 1052.
[39] P. Grassi, F. C. Drumm, J. Georgin, D. S. P. Franco, E. L. Foletto, G. L. Dotto, S. L. Jahn, *Environ. Technol. Innovation* **2020**, *17*, 100544.
[40] F. C. Drumm, J. S. d. Oliveira, E. L. Foletto, G. L. Dotto, E. M. M. Flores, M. S. P. Enders, E. I. Müller, S. L. Janh, *Chem. Eng. Commun.* **2018**, *205*, 445.
[41] J. S. d. Oliveira, M. A. Mazutti, E. A. Urquieta-González, E. L. Foletto, S. L. Jahn, *Mater. Res.* **2016**, *19*, 1399.
[42] M. Saleh, Z. Bilici, M. Kaya, M. Yalvac, H. Arslan, H. C. Yatmaz, N. Dizge, *Adv. Powder Technol.* **2021**, *32*, 1264.
[43] Y. S. Jung, W. T. Lim, J. Park, Y. Kim, *Environ. Technol.* **2009**, *30*, 183.
[44] C. d. Luca, P. Massa, J. M. Grau, S. G. Marchetti, R. Fenoglio, P. Haure, *Appl. Catal., B* **2018**, *237*, 1110.
[45] G. Busca, *Catal. Today* **2014**, *226*, 2.
[46] B. Kasprzyk-Hordern, M. Ziółek, J. Nawrocki, *Appl. Catal., B* **2003**, *46*, 639.
[47] A. Northup, D. Cassidy, *J. Hazard. Mater.* **2008**, *152*, 1164.
[48] H. Xu, T. Yu, X. Guo, J. Wang, *Desalin. Water Treat.* **2015**, *77*, 18028.
[49] A. P. Sarmento, A. C. Borges, A. T. de Matos, L. L. Romualdo, *Water* **2020**, *12*, 1655.
[50] T. D. Carlos, L. B. Bezerra, M. M. Vieira, R. A. Sarmento, D. H. Pereira, G. S. Cavallini, *J. Hazard. Mater.* **2021**, *403*, 123949.
[51] Y. Xiang, Y. Huang, B. Xiao, X. Wu, G. Zhang, *Appl. Surf. Sci.* **2020**, *513*, 145820.
[52] A. Elhalil, H. Tounsadi, R. Elmoubarki, F. Mahjoubi, M. Farnane, M. Sadiq, M. Abdennouri, S. Qourzal, N. Barka, *Water Resour. Ind.* **2016**, *15*, 41.
[53] K. C. Das, S. S. Dhar, *J. Alloys Compd.* **2020**, *828*, 154462.
[54] Y. Wu, S. Zeng, F. Wang, M. Megharaj, R. Naidu, Z. Chen, *Sep. Purif. Technol.* **2015**, *154*, 161.
[55] H. Meriem, D. Souad, T. Lakhdar, *J. Environ. Chem. Eng.* **2020**, *8*, 104457.
[56] C.-C. Chen, W.-C. Chen, M.-R. Chiou, S.-W. Chen, Y. Y. Chen, H.-J. Fan, *J. Hazard. Mater.* **2011**, *196*, 420.
[57] J. Wu, H. Gao, S. Yao, L. Chen, Y. Gao, H. Zhang, *Sep. Purif. Technol.* **2015**, *147*, 179.
[58] J. Chen, J. Feng, S. Lu, Z. Shen, Y. Du, L. Peng, P. Nian, S. Yuan, A. Zhang, *Sep. Purif. Technol.* **2018**, *191*, 75.
[59] Y. Xu, H. Shao, F. Ge, Y. Liu, *Chin. J. Catal.* **2017**, *37*, 1719.
[60] A. Khataee, P. Gholami, M. Sheydaei, *J. Taiwan Inst. Chem. Eng.* **2016**, *58*, 366.
[61] B. Kakavandi, A. Takdastan, S. Pourfadakari, M. Ahmadmoazzam, S. Jorfi, *J. Taiwan Inst. Chem. Eng.* **2019**, *96*, 329.